RESEARCH ARTICLE

Macromolecular Materials and Engineering
Open Access
www.mame-journal.de

Electrospun Fiber-Based Tubular Structures as 3D Scaffolds to Generate In Vitro Models for Small Intestine

*Lorenzo Zavagna, Eligio F. Canelli, Bahareh Azimi, Fabiola Troisi, Lorenzo Scarpelli, Teresa Macchi, Giuseppe Gallone, Massimiliano Labardi, Roberto Giovannoni, Mario Milazzo, and Serena Danti**

Recently, in vitro models emerge as valuable tools in biomedical research by enabling the investigation of complex physiological processes in a controlled environment, replicating some traits of interest of the biological tissues. This study focuses on the development of tubular polymeric scaffolds, made of electrospun fibers, aimed to generate three-dimensional (3D) in vitro intestinal models resembling the lumen of the gut. Polycaprolactone (PCL) and polyacrylonitrile (PAN) are used to produce tightly arranged ultrafine fiber meshes via electrospinning in the form of continuous tubular structures, mimicking the basement membrane on which the epithelial barrier is formed. Morphological, physical, mechanical, and piezoelectric properties of the PCL and PAN tubular scaffolds are investigated. They are cultured with Caco-2 cells using different biological coatings (i.e., collagen, gelatin, and fibrin) and their capability of promoting a compact epithelial layer is assessed. PCL and PAN scaffolds show 42% and 50% porosity, respectively, with pore diameters and size suitable to impede cell penetration, thus promoting an intestinal epithelial barrier formation. Even if both polymeric structures allow Caco-2 cell adhesion, PAN fiber meshes best suit many requirements needed by this model, including highest mechanical strength upon expansion, porosity and piezoelectric properties, along with the lowest pore size.

1. Introduction

The intestine stands as a vital component dedicated to the orchestration of nutrient intake, digestion and absorption from ingested sustenance, alongside the essential task of waste elimination, encompassing substances unmetabolized by the body. Serving as the key juncture between the internal milieu of the body and the external environment, it assumes a paramount role in safeguarding against the intrusion of detrimental substances and pathogens.[1] Moreover, the gut houses our microbiota; it strongly contributes to our immunity and exerts a bidirectional action towards the nervous system.[2]

Intestinal models serve as invaluable tools across diverse research domains by facilitating the exploration of substance bioavailability and bioactivity, as well as the study of intestinal pathology, such as the inflammatory bowel disease.[3] These models afford insights into the intricate processes of digestion, absorption and utilization of nutritional elements

L. Zavagna, B. Azimi, M. Milazzo, S. Danti
National Interuniversity Consortium for Materials Science and Technology (INSTM)
Florence 50121, Italy
E-mail: serena.danti@unipi.it
L. Zavagna
PEGASO Doctoral School of Life Sciences
University of Siena
Siena 53100, Italy

E. F. Canelli, B. Azimi, G. Gallone, M. Milazzo, S. Danti
Department of Civil and Industrial Engineering
University of Pisa
Largo Lucio Lazzarino 2, Pisa 56122, Italy
F. Troisi, R. Giovannoni
Department of Biology
University of Pisa
Pisa 56126, Italy
L. Scarpelli, M. Labardi, S. Danti
Institute for Chemical and Physical Processes (IPCF)
National Research Council (CNR)
Pisa Research Area, Pisa 56124, Italy
T. Macchi
Department of Translational Researches and New technologies in Medicine and Surgery
University of Pisa
Pisa 56126, Italy
R. Giovannoni, S. Danti
3R's Center
University of Pisa
Pisa 56100, Italy

The ORCID identification number(s) for the author(s) of this article can be found under https://doi.org/10.1002/mame.202400123

DOI: 10.1002/mame.202400123

within the body. Overall, they aim to shed light on gastrointestinal tract dynamics, the impact of ingested substances and disease conditions. Exploring factors influencing nutrient, drug and bioactive compound availability and functionality, these models can additionally elucidate interactions with intestinal cells and target tissues. Therefore, having intestine models available is pivotal in advancing our understanding of digestion, absorption and the development of effective therapeutic and nutritional strategies.[4,5] Over time, a plethora of intestinal models has emerged, each of them boasting unique complexities and characteristics, which offer distinct advantages and enable focused exploration of specific mechanisms.[6]

Animal models are widely employed to assess the absorption of drugs and food components; however, they come with inherent limitations. One significant challenge is the lack of a standard for comparing results due to individual variations and the complex networks and ecosystems within each animal. While these networks contribute to valuable preclinical trial outcomes, it is difficult to isolate each physiological process amidst the immense complexity and numerous variables of the system.[7] The ongoing issues of cost, time and ethical concerns associated with animal experiments further compound these challenges.[8]

To overcome these limitations, a surge in demand for specific in vitro models is taking place.[7] Cell-based models have emerged as promising alternatives to animal models by offering advantages such as direct observation, continuous analysis and target-specific experimentation.[6] In contrast to in vivo experiments, in vitro experiments can be meticulously designed to minimize deviations in the results by concentrating solely on specific elements of interest. Bidimensional (2D) cell-based models involve the cultivation of single or multiple cells on a flat surface. In the context of creating an intestinal model, specific cell lines are utilized to form an apical epithelial layer, with additional cell lines potentially incorporated for specialized functions. This model is characterized by its simplicity, cost-effectiveness and widespread application in screening assays, aimed at determining the bioavailability of orally administered drugs or assessing the absorption of substances found in food or nutraceuticals.[9] The Caco-2 cell line stands out as the most frequently utilized cell line in such models; although, alternative cells may be employed to enhance the model physiological resemblance to reality.[10] However, there are limitations associated with using 2D models of Caco-2 cells. For instance, 2D cultures inadequately replicate the physiological relevance of three-dimensional (3D) structures and interactions present in native tissues, leading to disparities in cellular behavior and function compared to in vivo observations. Therefore, it has become imperative to complement them with other models, such as 3D cell cultures or animal models.[11] In recent years, 3D cell culture in vitro models have gained significant popularity due to their ability to facilitate cell shape alterations and intercellular connections over time. These models have been crafted utilizing diverse techniques, including spontaneous aggregation, culture onto 3D scaffolds, or in a transwell setup, to offer a reproducible scenario for scientific and industrial investigations. Nevertheless, sustaining the vitality and bioactivity of cells over extended periods remains a critical challenge for these models.[12] To this purpose, the addition of bioactive molecules, such as extracellular matrix (ECM) proteins, to in vitro cellular models of Caco-2 cells has revealed still variegated outcomes, in terms of cell differentiation and transportation efficacy across the epithelial barrier.[13,14]

Significant advancements in this field of research have emerged through 3D fluid-dynamic in vitro models, which aim at offering a solution to the constraints of static cultures. These models can accurately replicate the intricate physiology of the human intestine by introducing essential physical stimuli, such as peristaltic loading; thus, recreating a dynamic microenvironment akin to the body. The incorporation of fluid flows and mechanical stimuli in these models has notably influenced gene expression profiles.[15] Notably, immortalized cell lines such as Caco-2 cells, known for their limitations in static conditions, can develop a compact intestinal epithelial layer featuring 3D villi-like structures and basal crypts when subjected to stimulation in a fluid-dynamic environment.[16] Unlike intestine-on-chip models for a macro-scale 3D model, cells need to be cultured onto 3D scaffolds to obtain the desired shape and function of the tissue.

There is a portfolio of biomaterials and processing techniques which can be useful for this purpose.[17] Electrospinning, a manufacturing technique with roots dating back to the late 19th century but gaining prominence in 1994, has emerged as a versatile method for producing fibrous structures with diverse applications.[18] Its strength lies in the ability to create scaffolds closely mimicking the ECM of tissues through the generation of sub-micrometric fibers.[19] This method offers numerous advantages, including generating scaffolds with a high surface area-to-volume ratio, a tunable porosity and the capacity to tailor nanofiber composition for desired properties and functions.[18] An essential advantage of electrospun scaffolds is an enhanced cell adhesion, crucial for various biomedical and tissue engineering applications. Indeed, the high surface area and unique topography of electrospun fibers promote cell attachment and proliferation. Moreover, precise control over electrospinning parameters can yield fibrous structures with specific fiber and mesh features, further influencing cell behavior and tissue organization.[20] Over time, a wide array of polymers has been processed via electrospinning, thus facilitating exploration across diverse fields, such as regenerative medicine, drug delivery, filtration and sensors. Each polymer offers specific properties by enhancing the versatility and potential of electrospinning as a fabrication technique.[18] Recently, electrospun polymeric scaffolds have been investigated to create epithelial intestine models for pathologic gut, such as colorectal adenocarcinoma.[21] Among polylactic acid and polycaprolactone (PCL) fibrous meshes, PCL scaffolds produced by electrospinning a chloroform solution with a random-like disposition, disclosed potential to suit the mechanical properties of human large intestine and support growth of Caco-2 cells. However, scaffolds made of PCL fibers collected using a drum rotating at at 500 revolutions per minute (rpm) showed large diameters and pore size in the 26–30 µm range, which

R. Giovannoni
Interdepartmental Research Center in Nutraceuticals and Food for Health (NUTRAFOOD)
University of Pisa
Pisa 56126, Italy

allowed cell infiltration within the scaffold. As such, this scaffold cannot be suitable to generate a model of intestinal epithelial barrier.

In view of providing a 3D in vitro model able to resemble the intestine epithelial barrier, which would be relevant for a real-scale dynamic system, this study aims at developing continuous tubular structures made of ultrafine polymeric fiber meshes with low pore size and high porosity to impose Caco-2 cells to colonize only the top layer of the scaffolds. The features mentioned above would ensure the formation of a compact layer of intestinal epithelial cells, which might be capable of nutrient exchanges across the fibrous membrane thickness. This investigation reports on the design and the fabrication, as well as on the morphological, physical, piezoelectrical and mechanical characterization of tubular structures made of nonwoven PCL and polyacrylonitrile (PAN) ultrafine fibers, the latter chosen for its piezoelectric properties, which may offer valuable stimuli for intestinal cells. Finally, we show the ability of these scaffolds to generate 3D in vitro models of small intestine epithelia by culturing them with Caco-2 cells using three different coating proteins (i.e., gelatin, collagen type I and fibrin) and by studying the morphological features of the formed cellular layer.

2. Experimental Section

2.1. Materials

PCL in the form of 3 mm grains, M_n of 80 kDa, and density of 1.145 g cm^{-3} was purchased from Sigma–Aldrich (St. Louis, Missouri, USA). PAN in powder form, with average M_w of 150 kDa and density of 1.184 g cm^{-3}, was purchased from BIOSYNTH (Staad, Switzerland). Chloroform ($CHCl_3$) and tetrahydrofuran (THF) were supplied by VWR Chemicals (Radnor, PA, USA); while, Dimethylformammide (DMF) was purchased from Sigma–Aldrich. Human colon adenocarcinoma tumoral cells (Caco-2) were purchased from ATCC (American type culture collection, Manassas, VA, USA). Fetal bovine serum (FBS), Live/Dead kits, Floromount-G, primary polyclonal anti-rabbit antibody ZO-1, HEPES 1 mM, DAPI (product code: D1306), and RNA Mini Kit were purchased from Invitrogen by Life Technologies Thermo Fisher Scientific (Waltham, MA, USA). Resazurin, Eagle' Minimum Essential Medium (EMEM), Sudan Black, Triton X-100, fibrinogen and thrombin were obtained from Sigma–Aldrich via Merck (Darmstadt, Germany). Levofloxacin was purchased from Fresenius Kabi (Vicchio, FI, Italy). Fluconazole was supplied by Bioindustria L.I.M. (Novi Ligure, AL, Italy). Neutral buffered formalin (product code: 0501004F) was purchased from Bio-Optica, Milan, Italy. Phalloidin-iFluor 488 conjugate (product code: ab176753) was bought from Abcam (Cambridge, MA, USA). Collagen type I (MAPTrix-C) was purchased from AMSBIO (Abingdon, England). Biotinylated goat anti-rabbit secondary antibody (product code: BA-9200) and goat serum were purchased from Vector Laboratories (Burlingame, CA, USA). PureLink RNA Mini Kit, SuperScript IV VILO Master Mix, ezDNase buffer, nuclease-free water, PowerUp SYBR Green Master Mix and SYBR Green PCR Master Mix were supplied by Thermo Fisher Scientific (Waltham, MA, USA).

2.2. Fabrication of the Tubular Scaffolds

The PCL solution was prepared with a concentration of 15% w/v in a THF/DMF mixture (1:1 w/w); while, the PAN solution was prepared with a concentration of 15% w/v in DMF by magnetic stirring at 300 rpm overnight at room temperature. Solutions were kept under gentle stirring at room temperature prior to usage.

Electrospinning was performed within a horizontal set-up using the Starter Kit-Aligned 1 (Linari Engineering s.r.l., Pisa, Italy), including a 5 mL glass syringe equipped with a G21 stainless steel blunt tip needle, placed on a syringe pump controlling the flow rate of the polymer solution. The fibers were spun on a stainless-steel rotating cylindrical collector (diameter of 7.4 mm and height of 100 mm) covered with an aluminum foil. The PCL solution was processed using the following parameters: flow rate of 1 mL h^{-1}, applied voltage of 12 kV, distance between syringe and collector set to 18 cm and collector speed of 5 rpm. The electrospinning time was 20 min. For the PAN solution, the electrospinning parameters were set to: flow rate of 0.25 mL h^{-1}, applied voltage of 12.5 kV, needle-collector distance of 15 cm and collector speed of 5 rpm. Electrospinning time was set to 40 min. In all cases, the fabricated tubular scaffolds possessed a thickness of ≈0.1 mm. All electrospinning parameters are summarized in **Table 1**.

2.3. Morphological Characterization of the Tubular Scaffolds

The morphological analysis of the fibers was performed by field emission scanning electron microscopy (SEM) using a Phenom Pro Desktop apparatus by Thermo Fisher Scientific (Milan, IT). Prior to observation, the samples were sputter-coated with gold with a S150B Sputter Coater by Edwards High Vacuum International (West Sussex, UK). Fiber diameters and porosity were measured with ImageJ software (version 1.54f, National Institute of Health, USA). Pore equivalent diameters were obtained from the measured areas by assuming the pores to be circles. Distinct fibers were measured to obtain mean diameters and diameter distributions ($n = 100$). Porosity analysis was performed by first adjusting the colour threshold to obtain a clear image of the first two fiber layers; and then, applying the "Analyze Particles" measurement tool.

2.4. Mechanical Characterization of the Tubular Scaffolds

The mechanical characterization of the tubular scaffolds was performed under radial expansion mode to resemble some traits of intestinal peristalsis. It was evaluated by means of a dedicated set-up, designed and assembled to measure the radial deformation of the tubular structure as a function of the measured internal pressure (Figure S1A, Supporting Information). The equipment consisted of three interconnected components that communicated with each other through a "Y" connector. The components included a sphygmomanometer pump with a check valve, used to pump air into the circuit, a manometer with a sensitivity of 1 mmHg to monitor the pressure, and a catheter with a spherical deformable part on which the tubular scaffolds were positioned (Figure S1B,C, Supporting Information). To

Table 1. Summary of process parameters used for electrospinning.

Polymer	Solvent(s)	Solution concentration [w/v%]	Flow rate [mL h^{-1}]	Needle-collector distance [cm]	Voltage [kV]	Rotational speed [rpm]
PCL	DFM/THF 50/50 [v/v]	15	1.00	18	12.0	5
PAN	DMF	15	0.25	15	12.5	5

accurately determine the radial deformation of the catheter, and consequently, the deformation of the tubular scaffold, a graduated glass cylinder with a sensitivity of 0.1 mL was used, in which the scaffold-catheter assembly was immersed (Figure S1D, Supporting Information). By measuring the increment of volume as an increment of the spherical part of the catheter, the increase of the radii as a function of the applied pressure was determined.

2.5. Wettability of the Scaffolds

Circular flat samples were cut from the tubular speciemens via an 8 mm-diameter dermal puncherand used to measure the static water contact angle (WCA). Drops of 3 µL of distilled water were placed on the samples using a micropipette, and WCA was obtained by means of a custom-made instrument (Linari Engineering s.r.l.) consisting of a DC-powered motor with a rotational speed varying from 1 rpm to 600 rpm and a camera with a 40-fps frame rate. ImageJ software was used for post-processing the acquired images analysis.

2.6. Piezoelectric Properties of the Scaffolds

The measurements of the d_{31} piezoelectric coefficient of the produced meshes were conducted using a PiezoGauge setup specifically developed for measuring the piezoelectric values of the meshes at a macroscale level, as detailed in prior work.[22] This setup involves clamping a stripe of the nanofiber mesh between a rigid support and a flexible steel cantilever, which serves as a sensitive force gauge. An electric field was thus applied orthogonally to the mesh thickness by electrically biasing two parallel metal plates. The resulting cantilever bending, induced by the piezoelectric stress of the mesh, was detected using the optical lever method. To enhance measurement precision, an alternating current (AC) electrics field was applied at the resonant frequency of the steel cantilever, typically around 150 Hz. This method led to an amplification effect of ≈20–30 times, resulting in a significant enhancement of measurement sensitivity. Poled poly(vinylidene fluoride) (PVDF) GoodFellow film was used as a standard control; whereas, electrospun fibers of PVDF/$BaTiO_3$ and poly(ethylene oxide terephthalate)-poly(butylene terephthalate) (PEOT-PBT) were used as positive and negative control, respectively.[22]

2.7. Cell Cultures on Fiber Meshes

The scaffolds, 8 mm diameter discs ($n = 6$), were sterilized by 97% v/v% ethanol/water overnight, followed by three washings of sterile saline solution added with 10% antibiotic (Levofloxacin) and 10% antimycotic (Fluconazole). The Caco-2 cells were cultured in 75 cm^2 tissue culture flasks using EMEM supplemented with 1% penicillin–streptomycin, 1% L-glutamine, and 10% FBS in a humidified incubator set at 37 °C with 95% air and 5% CO_2. When about 80% confluence was reached, the cells were detached via trypsin and counted. Caco-2 cells were seeded with a density of 1.5×10^5 cells cm^{-2} using the following treatments for scaffold coating:

(a) The first is gelatin (bovine). Cells were suspended in a 2% gelatin/PBS solution and seeded in droplets at the center of the dish. After a 30-min incubation period, the culture medium was added.

(b) The second is collagen type I (recombinant). The collagen solution was prepared by mixing inside an ice-cooled Eppendorf tube with 1 M HEPES, a solution of 37 g L^{-1} of $NaHCO_3$ and 5 mg mL^{-1} collagen type I, in a 1:1:8 ratio. A total of 150 µL of this solution was then added to each sample, and subsequently, the plate was placed in an incubator to allow the collagen to gel. After 30 min, the cells were seeded onto the coated samples.

(c) The third is fibrin (bovine). Fibrinogen was dissolved by gently mixing it in a saline solution at 37 °C to obtain a concentration of 4 mg m L^{-1}. Then, 1 mg of thrombin was dissolved in 1 mL of sterile water to create a solution with a concentration of 144 U mL^{-1}. The thrombin solution was further diluted in 25 mM $CaCl_2$ to achieve a concentration of 10 U mL^{-1}. Cells were suspended in the thrombin solution; therefore, thrombin and fibrinogen were mixed in a 1:1 ratio to form the fibrin clot. In our case, the clots were obtained by mixing 10 µL of thrombin with 10 µL of fibrinogen, resulting in 20 µL droplets, one for each fiber disk. The droplet took ≈30 s to coagulate, after which they were incubated for 30 min before adding the culture medium.

All the cultivated dishes were placed in a well of a 48-well plate. The samples were thus incubated for 1 h to ensure cell adhesion. Afterward, the specimens were completely covered by complete medium and cultured for 21 days by replacing the medium every 3 days.

Cell culture was also conducted on PCL and PAN tubular structures (5 mm high and 8 mm diameter) ($n = 6$) by seeding Caco-2 cells at 1.5×10^5 cells cm^{-2}. Before starting the experiments, the tubes were sterilized as reported above. Collagen type I and fibrin were used as coatings due to their capacity of gelation, which resulted in better suitability to entrap the cells onto these nonplanar scaffolds. For each scaffold, four 20 µL drops were placed on each quarter of the anulus after 90° rotation, with a time interval of 20 min between each drop to give the cells enough time to adhere to the scaffold. After the last drop, the scaffolds were

left in a cell culture incubator for 30 min, and then, the complete medium was added. The culture of tubular scaffolds was carried out for 8 days.

2.8. Cell Viability on the Scaffolds

The Alamar Blue viability assay was performed to monitor the metabolic activity of the cells. A 0.01% w/v% resazurin/EMEM solution was prepared. Then, 1 mL of this solution was added to each well containing the cell/scaffold constructs, as well as to other empty wells for control purposes. The cells were incubated for 3 h, after which, three 100 µL aliquots were taken from each well and transferred to a 96-well plate for spectrophotometric reading using the Victor 3 Multiplate Reader (PerkinElmer, Waltham, MA, USA).

Live/dead assays were performed at the end of cell cultures on planar scaffolds. For this assay, 1 mL sterile PBS solution containing 1 µL Calcein AM and 0.5 µL ethidium homodimer-1 was added to each well containing seeded fibers. Therefore, after 30 min in the incubator, samples were observed under an inverted fluorescence microscope (Nikon Ti, Amsterdam, The Netherlands).

2.9. Morphological Analysis of Cell/Scaffold Constructs

At the end of the culture, the cellular samples were fixed in 1% w/v% neutral buffered formalin for 10 min at 4 °C. The samples were washed in 1× PBS, and then, permeabilized by incubation in 0.1% Triton X-100 diluted in 1× PBS for 5 min. Then, they were immersed for 30 min in a Sudan black solution (0.3% w/v%) to cover the autofluorescence of the protein-coated fibers. After rinsing in PBS, they were treated with 1% eosin in water for 1 min and with DAPI solution (10 µg mL^{-1}) for 10 min. The results were observed with an inverted microscope equipped for the fluorescence and with a Nikon Eclipse Ti digital camera (Nikon Instruments).

Fixed cell/scaffold constructs were used for SEM analysis. After washings the samples in 1× PBS, they were immersed in a series of water/ethanol solutions with increasing ethanol concentrations: 70%, 80%, 90%, 95%, and 99% v/v%, for a duration of 15 min each, and then, fully dehydrated in a vacuum woven at 37 °C overnight. The dried samples were analyzed as reported in Section 2.3.

2.10. Gene Expression Analysis

The RNA extraction from Caco-2 cell cultured on PAN and PCL scaffolds with gelatin, collagen, and fibrin coatings for 21 days, including cells seeded with the same cellular density per surface area on Transwells (with and without collagen coating), was performed using the PureLink RNA Mini Kit following the manufacturer's protocol. Initially, the cells were lyzed in the lysis buffer and homogenized using a Dounce homogenizer; while, keeping the tube on ice throughout the procedure. The nucleic acids were then precipitated by adding ethanol to the lysis buffer, and the resulting solution was loaded onto a column for RNA binding, washing, and final elution in RNase-free water. For reverse transcription, a total volume of 10 µL was prepared in a RNase-free tube. The process involved adding the following components: 10× ezDNase buffer, ezDNase, template RNA, and nuclease-free water. The tube was centrifuged to collect all the solution at the bottom, and the samples were incubated at 37 °C for 2 min. After brief centrifugation and placing the tubes on ice, the following reagents were added: SuperScript IV VILO Master Mix (4 µL) and Nuclease-free water (6 µL). The reaction mix was then subjected to thermal cycling with the following conditions: 25 °C for 10 min, 50 °C for 10 min, and 85 °C for 5 min. The obtained cDNA product was subsequently used for real-time PCR and carried out using the PowerUp SYBR Green Master Mix. In a polypropylene tube, a PCR reagent mixture was prepared, consisting of Power SYBR Green PCR Master Mix (1×), reverse primer (300 nM final concentration), forward primer (300 nM final concentration), and nuclease-free water (5 µL). To this mixture, 1 µL of template cDNA (0.1 ng) was added, resulting in a final volume of 20 µL. Subsequently, the 96-well plate was inserted into the thermal cycler and subjected to the thermal cycling conditions reported in **Table 2**. The primers of ZO-1, Ezrin, and Occludin genes were designed using the "Primer3 Plus" tool.[23] The used PCR conditions are reported in Table 2. The experiments were performed in duplicate ($n = 2$).

Table 2. RT-PCR conditions.

Step	AmpliTaqgold enzyme activation	PCR (40 cycles)	
	Hold	Denature	Anneal/extend
Time	10 min	15 s	60 s
Temperature [°C]	95	95	60

2.11. Immunohistochemistry

Immunohistochemistry was performed directly on the scaffolds. After washing twice, the samples in 1× PBS for 5 min, the cell/scaffold constructs were permeabilized by 0.2% v/v% Triton X-100 in 1× PBS for 10 min and washed twice in 1× PBS for 5 min. Quenching of endogenous peroxidases was performed by incubation with 0.6% of 36 vol. H_2O_2 in methanol for 15 min in the dark. After washing in 1× PBS for 10 min, the samples were incubated with 5% v/v% goat serum diluted in 1× PBS for 20 min to block a-specific binding sites of the secondary antibody. After washing in 1× PBS for 5 min, the samples were incubated with primary polyclonal anti-rabbit antibody ZO-1 diluted in 0.1% w/v BSA/1× PBS (final concentration 2 mg mL^{-1}) in a moist chamber at 4 °C overnight.

Negative controls were performed incubating samples with 0.1% w/v BSA/1× PBS solution only. The following day, the specimens were incubated with goat anti-rabbit biotinylated secondary antibody diluted 1:200 in 1.5% v/v% goat serum/1× PBS solution for 60 min. Then, after washing twice, the samples in 1× PBS for 5 min, a streptavidin solution was added to the samples for 30 min, prepared according to manufacturer's instructions.

To reveal the reaction, after washing twice, the samples in 1× PBS for 5 min, they were incubated in the substrate-

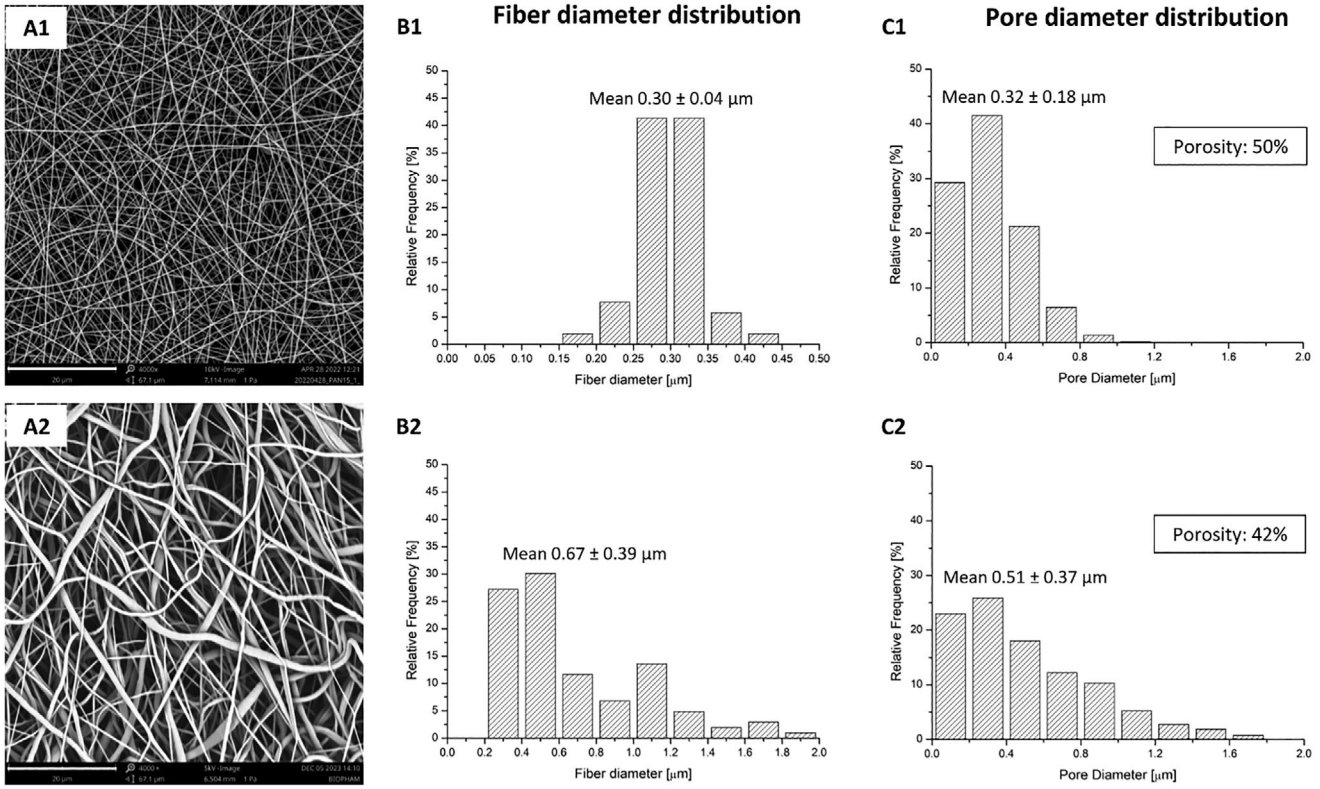

Figure 1. Results of morphological characterization of i) PAN (upper raw) and ii) PCL (lower raw) fiber meshes: A) SEM micrographs of the ultrafine fibers, scale bar: 20 µm. B) Bar graphs showing the fiber diameter distribution. C) Bar graphs showing the pore diameter distribution, calculated as a circle equivalent diameter from the pore areas.

chromogen solution: polyclonal antibody 0.5 mg mL^{-1} of 3,3'-Diaminobenzidine tetrahydrochloride activated with 1% of 36 vol. H_2O_2 (20 mL for each mL of DAB) for 5 min in the dark. The samples were then counterstained with Mayer's hematoxylin for 1 min and washed in tap water for 1 min. Finally, constructs were prepared with the Fluoromount mounting medium and observed with a Nikon Ti Eclipse inverted microscope equipped with a digital camera.

2.12. Statistical Analysis

Measures are reported as mean ± standard deviation. Statistical analysis was carried out to discuss the significance of the differences observed between the different scaffold groups. Independent *t*-test analyses were performed using Jamovi Software (version 2.2.5), taking account of the numerosity of the samples and setting a significance probability threshold (p) equal to 0.05 with an appropriate Bonferroni correction.

3. Results

3.1. Scaffold Characterization

PCL and PAN tubular scaffolds were produced with a diameter of 8 mm (Figure S2, Supporting Information). The morphological characterization of the fibrous is reported in **Figure 1**. Fiber size was different between the two polymers (Figure 1A1,A2). Image analysis revealed that electrospun PAN fibers had a mean diameter of 0.30 ± 0.04 µm; instead, electrospun PCL fibers showed a broader diameter distribution, with a mean value of 0.67 ± 0.39 µm (Figure 1B1,B2). Pore equivalent diameters of PAN and PCL meshes were 0.32 ± 0.18 µm and 0.51 ± 0.37 µm, and their average porosities were 50% and 42%, respectively (Figure 1C1,C2). Both PAN and PCL meshes displayed an appreciable porosity, that is, 50% and 42%, and pore size of 0.8 and 2.0 μm^2, respectively (Figure S3, Supporting Information).

The mechanical properties of the tubular scaffolds under radial expansion were obtained via a system that was designed and created to measure the deformation of the fibrous mesh structure as a function of the internal pressure (Figure S1, Supporting Information). The PAN scaffold resulted in less deformability than the PCL one; and therefore, in more resistance for pressures above 150 mmHg. Upon an inner expansion leading to a 18.1% circumferential deformation, the PAN tubular scaffolds were able to hold 42% higher pressure (i.e., 289 mmHg) than PCL ones (i.e., 203 mmHg). **Figure 2**A reports a graph of the experimental results, which were also solutions of cubic polynomial equations, reported as dotted lines. The measurement data are reported in **Table 3**.

The two polymers gave rise to fibrous meshes with different wettabilities, measured as WCAs, being PCL hydrophobic (WCA = 129° ± 21°) (Figure 2B) and PAN hydrophilic (WCA = 20° ± 6°) (Figure 2C). Measurements of the piezoelectric coefficients of

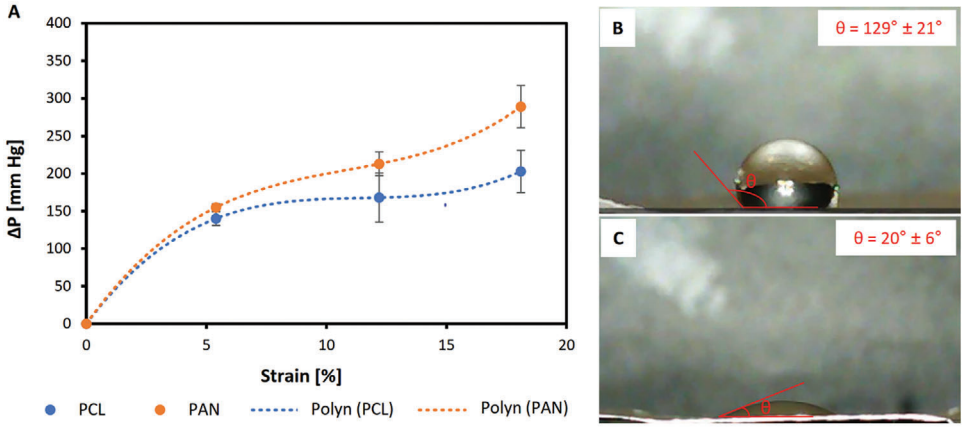

Figure 2. Results of mechanical and physical characterization of PAN and PCL tubular fibrous structures: A) Point graph showing the inner pressure difference [mmHg] held by the scaffolds as a function of deformation (%). Cubic polynomial equation displays the trend of the measured values. B,C) Representative photographs showing distilled water drops onto PCL (B) and PAN fiber meshes (C), used for WCA measurements.

the produced fiber meshes are reported in **Table 4**. PAN scaffolds showed a higher piezoelectric coefficient d_{31} = 20.0 ± 16.0 pm V^{-1} than PCL scaffolds (d_{31} = 1.12 ± 0.25 pm V^{-1}). The results presented in the table were obtained by averaging more than 20 values for each type of sample, obtained in different measurement conditions, that is, by using different samples, pretensions and measurements carried out on different days.

3.2. 3D Model Characterization

After 21 days, the Caco-2 cells were viable on all the coating/scaffold combinations, with metabolic cell activity on PAN scaffolds always overcoming that on PCL counterparts ($p < 0.001$ in gelatin- and collagen-coated scaffolds; $p < 0.0001$ in fibrin-coated scaffolds) (**Figure 3**). In PAN scaffolds, the highest metabolic activity was detected when the cells were cultured in the presence of gelatin and fibrin. Differently, in PCL, the highest metabolic activity was detected when the cells were cultured in the presence of gelatin and collagen. The morphological analysis was conducted at the endpoint via SEM and fluorescence microscopy. SEM micrographs revealed the formation of densely arranged cell layers on all the scaffold types (**Figure 4**). Collagen coatings specifically enabled the creation of a continuous layer of cells covering completely the outer surfaces of the fiber meshes (Figure 4B1,B2). In the other samples, but PAN/fibrin (Figure 4C2) in which the underlying fibers were well visible, the cell monolayers were well assembled even though they were possibly weaker than those shown in the collagen-covered scaffolds as several rifts or incompletely formed layers were observed (Figure 4A1,A2,C2).

The fluorescence microscopy outcomes are shown in **Figure 5** and confirmed the SEM observations. In addition, they display that the cell layer underneath the collagen-coated scaffolds had a morphology similar to those observed in all the other samples, thus corroborating the hypothesis that collagen was concurring to the compactness of the surface coating, as observed via SEM. The seeding technique reported in Section 2.7 allowed the annular-shaped scaffolds to be cultured with Caco-2 cells. Fibrin coating was used to this purpose due to the quicker gelation, which enabled the scaffolds under seeding to be rolled. In addition, under these experimental conditions, the Caco-2 cells were live and able to colonize both PAN and PCL scaffold surfaces (Figure S4, Supporting Information).

Gene expression analysis was performed after 21 culture days, including Caco-2 cells seeded with the same cellular density per surface area in Transwells (with and without collagen coating), used as standards in these experiments. The results are reported in **Figure 6**. We assessed the effect of the collagen and fibrin

Table 3. Outcomes of the mechanical measurements performed with the set-up in Figure S1, Supporting Information.

Circumferential strain [%]	Pressure [mmHg]	
	PCL	PAN
5.4	140 ± 9	155 ± 5
12.2	168 ± 33	213 ± 16
18.1	203 ± 28	289 ± 7

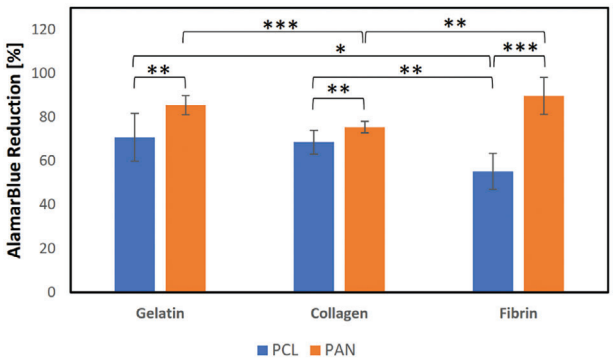

Figure 3. Bar graphs showing the outcomes of Caco-2 cell metabolic activity after 21-day culture on PCL or PAN scaffolds using three different coatings: gelatin, collagen and fibrin. Results are given as mean ± standard deviation; * $p < 0.05$, ** $p < 0.001$, and *** $p < 0.0001$.

Table 4. Results of the piezoelectric measurements of the fiber meshes.

Sample	PVDF GoodFellow (standard)	PVDF/$BaTiO_3$ (positive control)	PEOT-PBT (negative control)	PAN	PCL
Type	Film	Fiber meshes	Fiber meshes	Fiber meshes	Fiber meshes
ϵ_s	10.8	13.0	3.93	2.92	3.22
d_{31} [pm/V]	45 ± 6	65 ± 45	2.1 ± 1.7	20 ± 16	1.12 ± 0.25

PVDF: poly(vinylidene fluoride) and PEOT-PBT: poly(ethylene oxide terephthalate)-co-poly(butylene terephthalate).

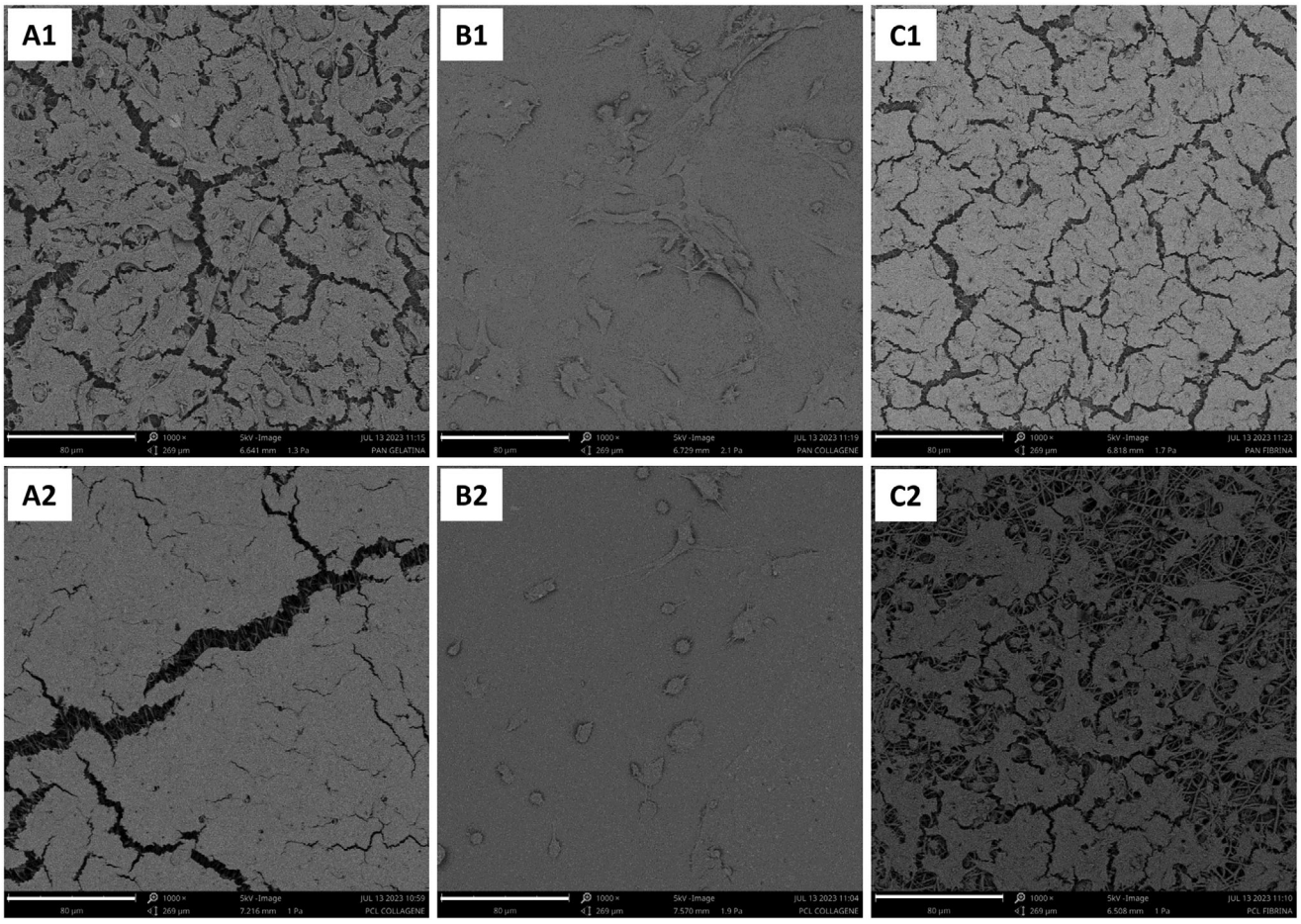

Figure 4. SEM micrographs showing the results of the morphological analysis of i) PAN (upper raw) and ii) PCL (lower row) scaffolds cultured with Caco-2 cells for 21 days by seeding the cells with three different protein coatings: A) gelatin, B) collagen and C) fibrin. Scale bar is 80 µm.

coating/scaffold systems developed in this study by considering gelatin coated scaffolds as reference samples.

The graph in Figure 6 shows that the cell culture on the scaffolds in the presence of collagen was able to increase the expression of Occludin both in PAN and PCL scaffolds, and at a lower extent also, of ZO-1 in PAN scaffold, with respect to gelatin coating and Transwell (with and without collagen coating). Moreover, fibrin-coated PAN scaffolds slightly improved the expression of Occludin. Differently, the highest Ezrin expression was found in the cells cultured on Transwells in the presence of collagen coating.

Figure 7 displays the outcomes of ZO-1 immunohistochemistry, performed directly on the top of the scaffolds provided with different coatings. A strong cell immunopositivity for ZO-1 was detected in all the samples, also confirming the cell colonization of the scaffolds. Moreover, the inserts of Figure 7, taken at high magnification, were able to show some traits of cell morphology on the different materials and coatings. In the presence of gelatin coating, most cells appeared to be surrounded, at least partially, by empty space, and displayed a mostly elongated morphology (Figure 7A). Differently, in the presence of collagen coating, the cells were in tight contact with each other by forming a continuous cell layer in most cases. Moreover, in these conditions, Caco-2 cells displayed a cubical-like morphology, altogether indicating the formation of monolayer structure (Figure 7B). Finally, in the presence of fibrin coating, the cells appeared to have a reduced size as compared to those observed in Figure 7B, thus suggesting an incomplete establishment of the monolayer structure.

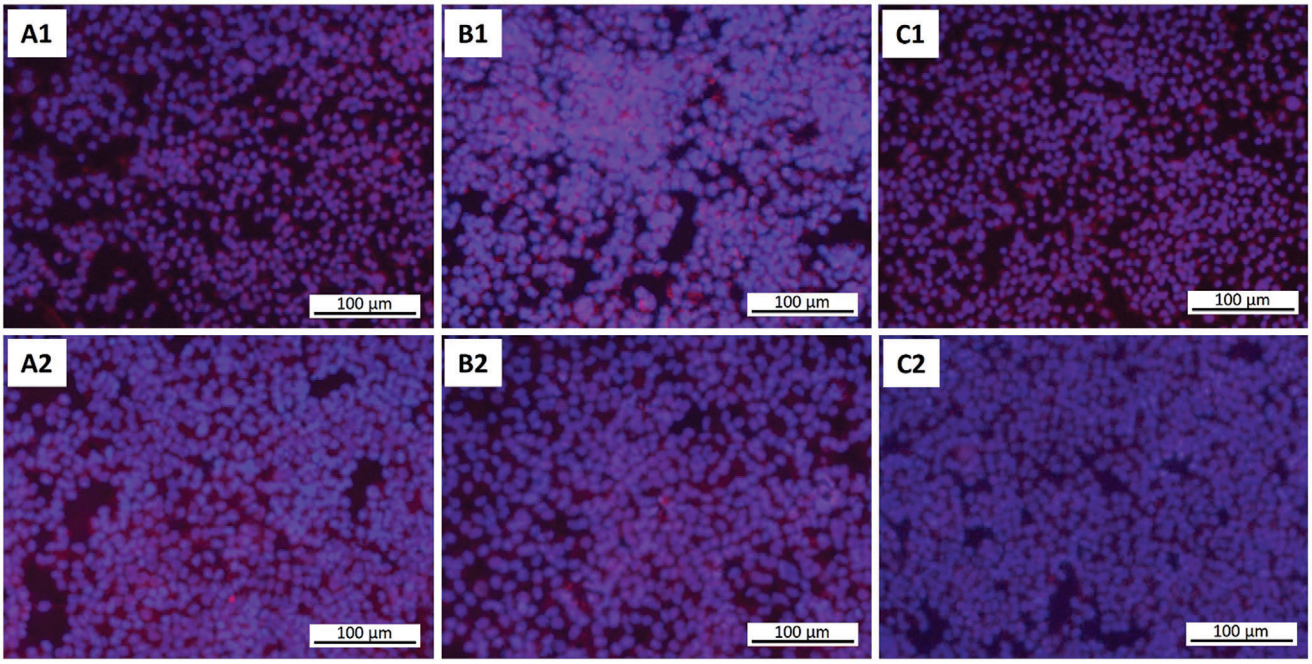

Figure 5. Fluorescence micrographs displaying results of the morphological analysis of i) PAN (upper raw) and ii) PCL (lower row) scaffolds cultured with Caco-2 cells for 21 days by seeding the cells with three different protein coatings: A) gelatin, B) collagen and C) fibrin. Nuclei are stained in blue and the cytoplasm is stained in pink. Scale bar is 100 µm.

4. Discussion

The small intestine operates food digestion in cooperation with billions of microbes inhabiting the intestinal lumen. This partnership occurs as the epithelial cell layer lining the lumen acts as a protective shield, safeguarding the body from direct contact with microbes and food antigens.[24] The importance of such a compact cellular layer is recognized to be crucial for health. Many disorders can indeed take place when the morphology and physiology of the intestinal barrier are compromised, including Inflammatory bowel diseases, irritable bowel and leaky gut syndromes, celiac disease, food allergies and sensitivities, as well as infectious gastroenteritis, which induces malabsorption of vital nutrients and erratic activation of the immune system.[25] Maintaining the integrity of the intestinal barrier is thus crucial for overall digestive health by preventing the onset of these

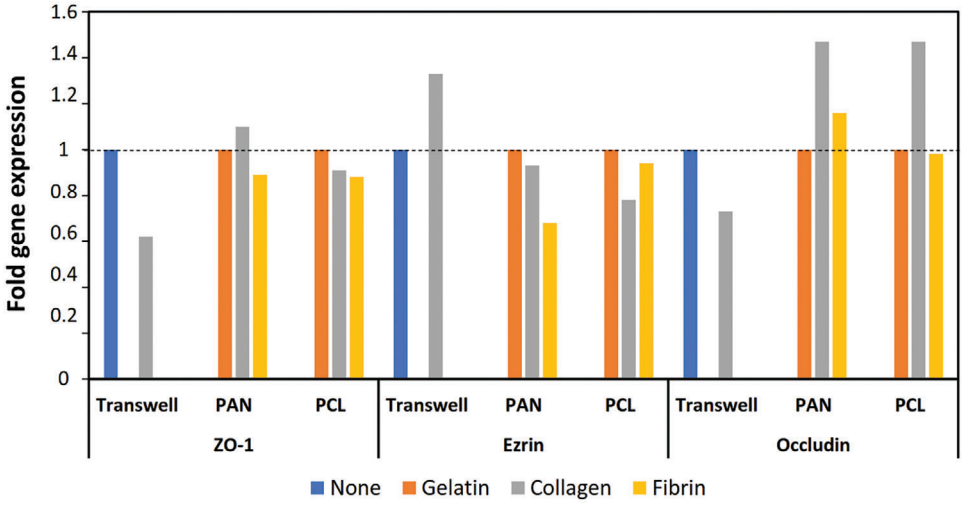

Figure 6. Results of RT-PCR conducted to evaluate the expression of ZO-1, Ezrin, and Occludin genes in Caco-2 cells after 21 culture days on PAN and PCL scaffolds coated with gelatin, collagen and fibrin. The experiments also included Caco-2 cells cultured on Transwells with and without collagen coating, considered as a standard 3D culture in this field. Gelatin and uncoated Transwells were used as test references for cells cultured on Transwells and scaffolds, respectively. The values were reported as averages of two independent samples ($n = 2$).

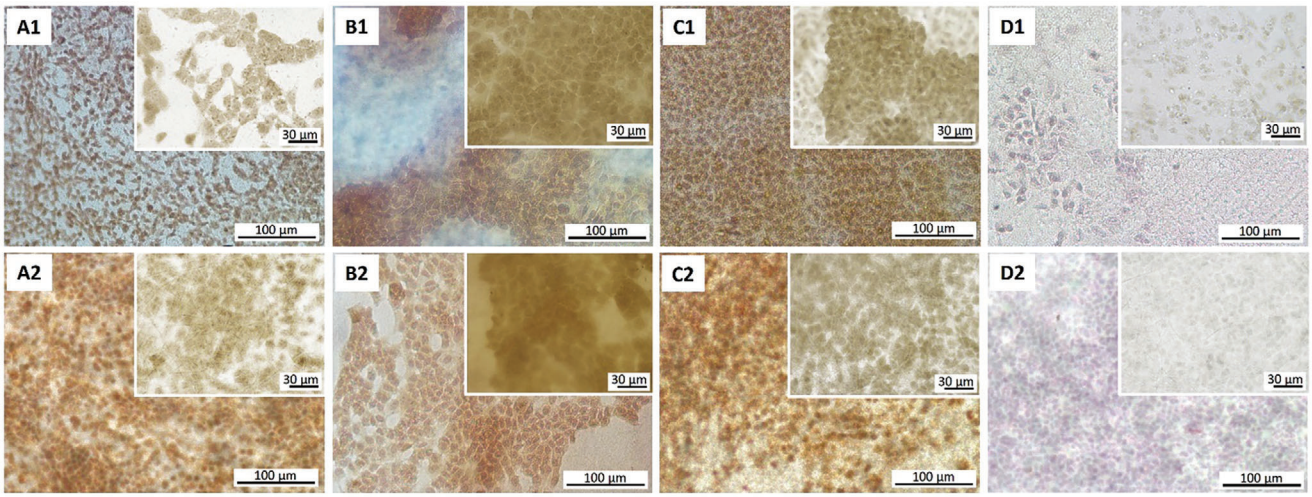

Figure 7. Micrographs showing the immunopositivity for ZO-1 of Caco-2 cells cultured for 21 days on i) PAN and ii) PCL scaffolds, coated with A) gelatin, B) collagen, and C) fibrin. D) Negative controls (fibrin-coated) of the immunohistochemical reaction (scale bar is 100 µm). Inserts show cellular morphology (600× total magnification; scale bar is 30 µm).

conditions. The research on the possible positive influence of drugs and nutraceuticals can largely benefit from in vitro intestine models, which however struggle to reproduce the complexity of the digestive environment, made up by biological, electrical and mechanical stimuli. Tissue engineering proposes to generate 3D in vitro models, which could leverage the replication of anatomic and physiologic features by developing appropriate biomaterial scaffolds on which the cells are cultured, as well as bioreactors to apply suitable mechanical forces onto them.[24] Due to the complexity of the biological microenvironment provided by the intestinal barrier, several studies are evaluating the prominent roles exerted by ECM molecules to generate accurate in vitro models.[26,27]

This study aims at developing tubular elements resembling the small intestine epithelial barrier produced via electrospinning. This electrodynamic technology is widely used to produce scaffolds made of ultrafine polymer fibers, that is, with submicrometric size, which entails the mimicry of the fibrous ECM.[19] Such fiber nonwoven meshes can also find applications as filtering layers.[28] Both applications unveil the electrospinning potential of tuning the fiber features such as fiber diameters, pore size and porosity, which make this spinning technique unique to ultimately generate a substrate for intestine barrier.[29]

Intestinal epithelial cells can harness the advantages of isotropic random fiber scaffolds, leveraging scaffold topography as a critical determinant in cell adhesion. Fibrous scaffolds, derived from PCL alone or its blends with other polymers, have shown the ability to mimic the nanoscale topography akin to the basement membrane.[30] When crafting a porous membrane to create a tissue barrier properly resembling the basement membrane for supporting epithelia, a multitude of scaffold characteristics demands attention to enhance the biomimetic physiological fidelity. Among these, pore size emerges as a pivotal consideration, dictating whether cells primarily engage with the surface (<1 µm), foster intercellular communication (1–3 µm), or traverse the membrane/scaffold (3–12 µm). The pore dimensions measuring less than 2 μm^2 prove insufficient access for cellular transmigration into the scaffold.[31] This evidence underscores that cells are likely to develop as monolayers atop such membranes, with limited penetration into the biomaterial structure; thus, aligning with the intended design intent for intestinal epithelial barrier scaffolds.

In our study, we selected two polymer types used in the biomedical sector, namely, PAN and PCL, potentially suited for this application. PAN is a vinyl polymer characterized by each repeating unit containing a cyano (—CN) group, largely used to produce so-called "acrylic fibers," which have shown relevant mechanical properties, unique in textile and advanced applications, and in the latter, used as precursors for carbonization or graphitization processes, ultimately leading to carbon fibers.[32] PAN can be electrospun into ultrafine fibers, which are proposed for bone regeneration.[33] The chemical structure of PAN enables interesting piezoelectric properties, which can play a role in delivering biosignals to the proposed 3D in vitro model of an intestine barrier. In fact, the —CN functional group boasts a substantial dipole moment of 3.5 D, originating from the disparity in electron density between the carbon and nitrogen atoms, in which carbon is electron-deficient, whereas nitrogen is electron-rich.[34]

PCL is a long-term biodegradable polyester entitled with very high flexibility, an exceptional elongation at break (300–1000%) and good tensile strength.[35] Ricci et al. proposed PCL fibers, electrospun from a solution in chloroform in a random-like form, obtained by using a collector rotating at 500 rpm rotational speed, to generate 3D models of colorectal adenocarcinoma.[21] Such PCL scaffolds were reported to have similar Young's modulus and strain at break to those of the large intestine and allowed the growth of Caco-2 cells. The morphological characterization of those fiber meshes showed 87.57% porosity, fiber size of 3.10 ± 0.12 µm and highly distributed pore diameters (mean 8.56 µm, maximum 30 µm). However, such features are not suited to reproduce the intestinal barrier because the cells penetrate inside the fibrous mesh without generating a compact cellular layer atop the surface. To achieve this fundamental property, in this study, PCL was electrospun by preparing a solution in a

DMF/THF solvent system, which allowed a considerable reduction of fiber diameter (0.67 ± 0.39 μm), pore diameter (0.51 ± 0.37 μm), pore size (mean value 2 μm^2, with 63% pores <2 μm^2) and porosity (42%) of the scaffolds. PAN, electrospun in DMF, gave rise to fiber meshes with reduced and tightly distributed fiber size (0.30 ± 0.04 μm), showing pores with diameters and size even smaller (0.32 ± 0.18 μm diameter, pore size mean value of 0.8 μm^2, with 90% pores <2 μm^2), while also displaying higher porosity (50%) than those of the PCL counterpart. Thus, the morphological features of the electrospun PAN fiber meshes fully attained the requirements of basement membrane scaffolds.

Optimal cell adhesion on polymeric surfaces has been documented within a WCA range of 40–70°.[36] Nonetheless, this outcome is subject to various influencing factors such as cell type, duration of incubation, environmental conditions, surface chemistry and topographical characteristics. PCL is a notably hydrophobic polymer due to its aliphatic chains; however, the presence of a submicrometric fiber structure, mimicking the ECM, is well documented not to hinder cell adhesive properties.[37] Wettability measurements performed on electrospun scaffolds revealed a strongly hydrophobic behavior with mean WCA of 129°. Differently, PAN scaffolds demonstrated a highly iodophilic behavior with mean WCA of 20°. Even though cell adhesion is a determinant for the generation of a compact epithelial layer, the underneath substrate should also possess the property of allowing filtration of nutrients operated by intestinal cells. Therefore, it is extremely relevant to have diverse options, in terms of wettability, for subsequent research aimed to study the function of the intestinal barrier.

To produce both PCL and PAN fiber meshes suitable to have radially expandable tubes; thus, mimicking the mechanics of the intestine lumen, a quasi-zero (i.e., 5 rpm) rotating velocity of the collector was chosen. This speed allowed the fabrication of completely anisotropic fiber structures. A mechanical characterization was performed by designing a dedicated set-up, in which the annular scaffolds were placed on a swellable catheter and inflated using a sphygmomanometer system. Subjected to an inner radial expansion, leading to 18.1% circumferential deformation, PAN tubular scaffolds sustained a 42% higher pressure (i.e., 289 mmHg) than PCL ones (i.e., 203 mmHg), which indicated the highest strength of PAN fiber meshes.

PAN has garnered significant interest in recent times due to its notable piezoelectric characteristics, particularly when utilized in electrospun meshes. We selected PAN in view of a future use of the developed tubular scaffolds in a bioreactor, as piezoelectric scaffolds can activate a transient dipole formation, able to deliver local electrical signals that can be sensed by the cells.[22] Our piezoelectric investigation, obtained by averaging more than 20 measurements for each polymer mesh type obtained in different measurement conditions (i.e., different samples, pretensions and measurements carried out on different days from mesh production) showed a high variation in PAN scaffolds. This fact can be associated with the various phenomena of surface interaction, relaxation and fiber rearrangement, dominant in anisotropic fiber meshes. Anyway, PAN fiber meshes resulted to be piezoelectric, having $d_{31} = 20 \pm 16$ pm/V, whereas PCL fiber meshes were non-piezoelectric, having 1.12 ± 0.25 pm V^{-1}.

Both PAN and PCL fiber meshes were able to sustain the growth of Caco-2 cells on their top surface. We applied three different protein coatings on the polymeric scaffolds, aimed to promote cell adhesiveness and the generation of a compact cell layer.[13,14] Gut basement membrane is made up of laminins, collagens (mainly type IV), proteoglycans, calcium binding proteins and other structural or adhesive proteins.[38] With the intent of promoting cell adhesion, while, minimizing cell loss during and after seeding, we selected recombinant collagen type I, able to form a gel within 20 min, gelatin type B, as a denaturized form of collagen still exposing collagen aminoacidic residues but unable to jellify at 37 °C, and finally, fibrin, obtained with a quick (i.e., 30 s) crosslinking of fibrinogen and thrombin. With all these protein coatings, almost compact Caco-2 cell layers were obtained after 21 days. To seed annular-shaped scaffolds, fibrin was selected as it could entrap the cells within complex tube-like scaffold shapes.[39] Collagen promoted the formation of a homogeneous and stable surface coating, as visible via SEM; although, the cellularized layer was similar to those observed in gelatin- and ibrin-coated samples under fluorescence microscopy, without appreciable difference between PAN and PCL substrates.

The presence of the protein used for the coating played a role in regulating the expression of specific genes, sometimes in combination with the polymer scaffold. We analyzed the expression of genes involved in the formation and function of tight junctions and microvilli, namely, ZO-1,[40] Occludin,[41] and Ezrin.[42] The function of tight junctions in regulating the passage of molecules between neighboring epithelial cells and ensuring epithelial integrity was well-established; yet, their involvement in physiological cell shedding remains ambiguous. These dynamic structures comprise a complex network of interacting proteins, indicating their potential role in facilitating cell shedding processes.[43] The tight junction protein, known as zonula occludens protein-1 (ZO-1), which has been demonstrated to impart structural integrity and impermeability to the junction, serves as a crucial link between Occludin and the actin cytoskeleton.[44] Consequently, ZO-1 is involved in the maintenance of intestine barrier function. Occludin is a transmembrane protein that regulates the permeability of epithelial and endothelial barriers; therefore, it is an essential component of the tight junctions.[45] Finally, Ezrin links the cell cytoskeleton and the plasma membrane, thus regulating its tension and affecting cell motility.[46]

Different from Transwell culture of Caco-2, in which Ezrin was upregulated, collagen was able to upregulate the expression of Occludin in PAN and PCL scaffolds. In a similar fashion, ZO-1 was upregulated in collagen-coated PAN scaffolds, but not in Transwell. These results indicated that, besides the specific protein coating, which in the case of collagen appeared to be long-lasting, the undelaying polymer scaffold may also affect gene expression. Finally, we performed immunohistochemistry on a representative protein of tight junctions, that is, ZO-1, which was revealed to be markedly expressed in all coating/scaffold conditions. By comparing gene expression results with immunohistochemical outcomes, taken at the same time-point (i.e., 21 days), it appeared that ZO-1 and Ezrin gene expression levels were similar in all the scaffold/coating conditions. On the other hand, Occludin gene expression was found to be upregulated only in PAN and PCL scaffolds coated with collagen, in which a Caco-2

cell morphology coherent with the monolayer structure was observed.

Overall, the obtained findings suggest that it is possible to fabricate tubular electrospun scaffolds acting as basement membrane for the generation of intestine epithelium, ultimately, creating real-shape 3D in vitro models for the small intestine with potential to be used within a customized bioreactor, able to expand the tube, and mimic some features of peristaltic motion. These models could support the study of cell-nutrient or nutraceutical interactions when the barrier is compromised by stressing factors. Among the two polymeric structures investigated, PAN scaffolds offered better suited properties than PCL counterparts, such as smaller pore size (i.e., 90% of pores within 2 μm^2), higher mechanical strength upon radial expansion and appreciable piezoelectric properties; the latter potentially able to deliver local electric signals upon mechanical deformation, as present in the intestine tissue.[47] Caco-2 cells showed an increased metabolic activity on PAN scaffolds, with respect to PCL ones, independently of the protein coating applied. Coating with proteins could also be a successful strategy to enhance the formation of tight junctions by Caco-2 cell layers. Interestingly, PAN and PCL fibrous meshes offered an opposite behavior in terms of wettability, which did not prevent cell adhesion but could influence the filtration mechanism operated by the intestine barrier and a filtrate retention under the scaffold layer. This aspect needs to be investigated in future studies, aimed at assessing the function of the proposed in vitro model; thus, disclosing if the highly hydrophilic behavior of PAN should be modulated with the addition of a hydrophobic polymer, such as PCL. Having real-shape in vitro models available can promote the research in bowel diseases and development of targeted therapies.

5. Conclusion

This study explored the fabrication by electrospinning of polymeric scaffolds made of tightly arranged ultrafine fibers in the form of tubular structures to obtain real-shape 3D in vitro model of the small intestine in which nutrient absorption takes place. PAN and PCL were employed to this purpose. We characterized these scaffolds in terms of morphological, physical, mechanical and piezoelectric properties. By comparing the two scaffolds, PAN most properly attained the requirements identified to obtain a substrate resembling the basement membrane, thus supporting the generation of a surface epithelial layer. Both polymeric fibrous meshes were coated with three proteins, namely, gelatin, collagen and ibrin, prior to culture with Caco-2 cells, which resulted viable for 21 days. By virtue of the fast jelling properties of fibrin, annular-shape scaffolds could be efficiently seeded. The used coatings, sometimes in combination with the polymer scaffolds, were able to affect the expression of genes involved in tight junction formation. ZO-1 protein was revealed in all the samples. Such results indicate the potential of these electrospun polymer scaffolds to support Caco-2 cell growth and assembly into an intestinal epithelial barrier model. Future biological studies, to be also conducted dynamically using bioreactors, should assess the role of these in vitro systems to further model intestine absorption function, in normal and pathologic conditions.

Supporting Information

Supporting Information is available from the Wiley Online Library or from the author.

Acknowledgements

The authors acknowledge Dr. Delfo D'Alessandro (University of Pisa) for his technical support to immunohistochemistry. Linari Engineering s.r.l. is greatly thanked for making available for this research the electrospinning setup, the WCA measurement equipment and the SEM. This study was funded by the Italian Ministry of University and Research (MIUR) under the framework Azione II del PON "Ricerca e Innovazione" 2014–2020, project "Sviluppo di nutraceutici da fonti naturali—BIONUTRA" (CUP B14I20001320005) to S.D., and by the National Recovery and Resilience Plan (NRRP, Mission 4 Component 2 Investment 1.3 – Call for proposals No. 341 of 15 March 2022 of Italian Ministry of University and Research funded by the European Union – NextGenerationEU), Project "ON Foods – Research and innovation network on food and nutrition Sustainability, Safety and Security – Working ON Foods" (code PE00000003, Concession Decree No. 1550 of 11 October 2022 adopted by the Italian Ministry of University and Research, CUP D93C22000890001) to R.G. The MIT-UNIPI project 2022 "sMall-caliber vAscular Grafts in pulsed-flow mIcrofluidiCs (MAGIC))" (MISTI funds) is acknowledged by M.M.

Conflict of Interest

The authors declare no conflict of interest.

Author Contributions

L.Z. and E.F.C. contributed equally to this work. L.Z. contributed to Investigation, Conceptualization, Visualization, and Writing original-draft preparation. E.F.C. contributed to Investigation, Conceptualization, Visualization, and Writing original-draft preparation. B.A. contributed to Methodology and Supervision. F.T. contributed to Investigation, Data curation, and Writing original-draft preparation. L.S. contributed to Investigation and Data curation. T.M. contributed to Investigation, Methodology, and Supervision. G.G. contributed to Conceptualization and Methodology. M.L. contributed to Conceptualization, Methodology, Supervision, and Resources. M.M. contributed to Methodology, Data curation, Writing original-draft preparation, and Supervision. R.G. contributed to Methodology, Supervision, and Resources. S.D. contributed to Resources, Project Administration, Funding Acquisition, and Writing original-draft. All authors have reviewed, edited, and approved the submitted version.

Data Availability Statement

The data that support the findings of this study are available on request from the corresponding author. The data are not publicly available due to privacy or ethical restrictions.

Keywords

Caco-2 cells, piezoelectric, polyacrylonitrile (PAN), polycaprolactone (PCL), ZO-1

Received: March 27, 2024
Revised: May 22, 2024
Published online: August 27, 2024

[1] J. T. Collins, A. Nguyen, M. Badireddy, StatPearls. edn, Treasure Isl., **2023**.
[2] M. Carabotti, A. Scirocco, M. A. Maselli, C. Severi, *Ann. Gastroenterol.* **2015**, *28*, 203.
[3] S. Rahman, M. Ghiboub, J. M. Donkers, E. van de Steeg, E. A. F. van Tol, T. B. M. Hakvoort, W. J. de Jonge, *Int. J. Mol. Sci.* **2021**, *22*, 13472.
[4] P. Etcheverry, M. A. Grusak, L. E. Fleige, *Front. Physiol.* **2012**, *3*, 31039.
[5] A. Guerra, L. Etienne-Mesmin, V. Livrelli, S. Denis, S. Blanquet-Diot, M. Alric, *Trends Biotechnol.* **2012**, *30*, 591.
[6] H. Yu, N. M. Hasan, J. G. In, M. K. Estes, O. Kovbasnjuk, N. C. Zachos, M. Donowitz, *Annu. Rev. Physiol.* **2017**, *79*, 291.
[7] P. Lu, C. P. Sodhi, H. Jia, S. Shaffiey, M. Good, M. F. Branca, D. J. Hackam, *Am. J. Physiol.* **2014**, *306*, G917.
[8] D. Knecht, P. Cholewińska, A. Jankowska-Mąkosa, K. Czyż, *Animals* **2020**, *10*, 527.
[9] A. Fedi, C. Vitale, G. Ponschin, S. Ayehunie, M. Fato, S. Scaglione, *J. Controlled Release* **2021**, *335*, 247.
[10] T. Takenaka, N. Harada, J. Kuze, M. Chiba, T. Iwao, T. Matsunaga, *J. Pharm. Sci.* **2016**, *105*, 915.
[11] M. H. Macedo, E. Martínez, C. C. Barrias, B. Sarmento, *Front. Bioeng. Biotechnol.* **2020**, *8*, 524018.
[12] R. Salerno-Goncalves, A. Fasano, M. B. Sztein, *Gastroenterology* **2011**, *141*, e18.
[13] S. C. Kirkland, *Br. J. Cancer* **2009**, *101*, 320.
[14] L. Wang, S. K. Murthy, G. A. Barabino, R. L. Carrier, *Biomaterials* **2010**, *31*, 7586.
[15] H. J. Kim, H. Li, J. J. Collins, D. E. Ingber, *Proc. Natl. Acad. Sci. U. S. A.* **2016**, *113*, E7.
[16] K. Pocock, L. Delon, V. Bala, S. Rao, C. Priest, C. Prestidge, B. Thierry, *ACS Biomater. Sci. Eng.* **2017**, *3*, 951.
[17] J.-W. Jang, K.-E. Min, C. Kim, J. Shin, J. Lee, S. Yi, *Int. J. Precis. Eng. Manuf.* **2023**, *24*, 511.
[18] N. Bhardwaj, S. C. Kundu, *Biotechnol. Adv.* **2010**, *28*, 325.
[19] Y. Su, M. S. Toftdal, A. Le Friec, M. Dong, X. Han, M. Chen, *Small Sci.* **2021**, *1*, 2100003.
[20] S. I. Jeong, M. D. Krebs, C. A. Bonino, S. A. Khan, E. Alsberg, *Macromol. Biosci.* **2010**, *10*, 934.
[21] C. Ricci, B. Azimi, L. Panariello, B. Antognoli, B. Cecchini, R. Rovelli, M. Rustembek, P. Cinelli, M. Milazzo, S. Danti, A. Lazzeri, *Int. J. Mol. Sci.* **2023**, *24*, 9443.
[22] C. Mota, M. Labardi, L. Trombi, L. Astolfi, M. D'Acunto, D. Puppi, G. Gallone, F. Chiellini, S. Berrettini, L. Bruschini, S. Danti, *Mater. Des.* **2017**, *122*, 206.
[23] A. Untergasser, H. Nijveen, X. Rao, T. Bisseling, R. Geurts, J. A. M. Leunissen, *Nucleic Acids Res.* **2007**, *35*, W71.
[24] M. Antfolk, K. B. Jensen, *Nat. Commun.* **2020**, *11*, 6244.
[25] M. Abdulla, N. Mohammed, *Biol.: Targets Ther.* **2022**, *2022*, 129.
[26] M. J. Haddad, W. Sztupecki, C. Delayre-Orthez, L. Rhazi, N. Barbezier, F. Depeint, P. M. Anton, *Int. J. Mol. Sci.* **2023**, *24*, 3595.
[27] P. Zhao, X. Li, Q. Fang, F. Wang, Q. Ao, X. Wang, X. Tian, H. Tong, S. Bai, J. Fan, *Regener. Biomater.* **2020**, *7*, 627.
[28] X. Qin, S. Subianto, in *Electrospun Nanofibers* (Ed: M. Afshari), Woodhead Publishing Series in Textiles, Elsevier, Amsterdam, the Netherlands **2017**, pp. 449–466.
[29] A. M. Gonçalves, F. Leal, A. Moreira, T. Schellhorn, V. H. Blahnová, S. Zeiringer, K. Vocetková, C. Tetyczka, A. Simaite, M. Buzgo, E. Roblegg, P. F. Costa, P. Ertl, E. Filová, Y. Kohl, *Adv. Nanobiomed. Res.* **2023**, *3*, 2200104.
[30] S. Ferraris, S. Spriano, A. C. Scalia, A. Cochis, L. Rimondini, I. Cruz-Maya, V. Guarino, A. Varesano, C. Vineis, *Polymers* **2020**, *12*, 2896.
[31] J. M. Ameer, A. K. Pr, N. Kasoju, *J. Funct. Biomater.* **2019**, *10*, 30.
[32] H. Ahn, J.-H. Wee, Y. M. Kim, W.-R. Yu, S.-Y. Yeo, *Polymers* **2021**, *13*, 1613.
[33] F. S. T. Mirakabad, S. Hosseinzadeh, H. A. Abbaszadeh, V. Zeighamian, M. S. Khoramgah, H. Ghanbarian, J. Ranjbari, B. Kazemi, *Iran. J. Pharm. Res.* **2021**, *20*, 385.
[34] H. Ueda, S. H. Carr, *Polym. J.* **1984**, *16*, 661.
[35] M. M. Reddy, S. Vivekanandhan, M. Misra, S. K. Bhatia, A. K. Mohanty, *Prog. Polym. Sci.* **2013**, *38*, 1653.
[36] S. M. Oliveira, N. M. Alves, J. F. Mano, *J. Adhes. Sci. Technol.* **2014**, *28*, 843.
[37] A. Azari, A. Golchin, M. M. Maymand, F. Mansouri, A. Ardeshirylajimi, *Adv. Pharm. Bull.* **2022**, *12*, 658.
[38] A. C. Y. Li, R. P. H. Thompson, *Br. Med. J.* **2003**, *56*, 885.
[39] C. Mota, M. Milazzo, D. Panetta, L. Trombi, V. Gramigna, P. A. Salvadori, S. Giannotti, L. Bruschini, C. Stefanini, L. Moroni, S. Berrettini, S. Danti, *J. Mater. Sci. Mater. Med.* **2018**, *29*, 1.
[40] Y. Guan, A. J. M. Watson, A. M. Marchiando, E. Bradford, L. Shen, J. R. Turner, M. H. Montrose, *Am. J. Physiol.* **2011**, *300*, C1404.
[41] Z. M. Slifer, A. T. Blikslager, *Int. J. Mol. Sci.* **2020**, *21*, 972.
[42] X. Yao, L. Cheng, J. G. Forte, *J. Biol. Chem.* **1996**, *271*, 7224.
[43] L. Shen, C. R. Weber, J. R. Turner, *J. Cell Biol.* **2008**, *181*, 683.
[44] A. S. Fanning, B. J. Jameson, L. A. Jesaitis, J. M. Anderson, *J. Biol. Chem.* **1998**, *273*, 29745.
[45] G. J. Feldman, J. M. Mullin, M. P. Ryan, *Adv. Drug Delivery Rev.* **2005**, *57*, 883.
[46] A. Vaheri, O. Carpén, L. Heiska, T. S. Helander, J. Jääskeläinen, P. Majander-Nordenswan, M. Sainio, T. Timonen, O. Turunen, *Curr. Opin. Cell Biol.* **1997**, *9*, 659.
[47] M. Montorsi, L. Zavagna, L. Scarpelli, B. Azimi, S. Capaccioli, S. Danti, M. Labardi, *Polymers* **2024**, *16*, 1305.

